Additional Losses of Inverter Fed Asynchronous Induction Machines of Traction Drives – Comparison of Modelling and Measurements

Erich Schmidt
Institute of Energy Systems and Electric Drives, Vienna University of Technology, Vienna, Austria
erich.schmidt@tuwien.ac.at

Florian Müllner, Harald Neudorfer
Traktionssysteme Austria, Wiener Neudorf, Austria

Abstract – Additional losses of asynchronous induction machines utilized in traction drives caused by the inverter have a great impact of the thermal behaviour of such machines. Therefore, an accurate modelling and evaluation of these additional losses is a very important task in particular with the initial design. Based on detailed measurement data from already built machines, a fast and reliable calculation method of these additional losses suitable for the initial design of new machines is presented based on equivalent circuits of the induction machine for each higher harmonic components of the terminal voltages applied by the inverter.

Keywords – Additional losses, Iron losses, Eddy current losses, Asynchronous machine, Induction machine

1. Introduction

The evaluation of additional losses of inverter fed asynchronous induction machines with design and operation is an important task for many years [1]–[4]. On the other hand, asynchronous induction machines used with traction drives of rail transportation vehicles have different design strategies compared against commonly used standard machines. Since such machines have a very high utilization additionally, accurate modelling and precalculation of the additional losses caused by the inverter are an important task with both tender phase as well as electromagnetic and thermal initial design of these machines. Thus, the main components of these additional losses are discussed based on the spectrum of the non-sinusoidal voltages supplied by the inverter. An important viewpoint of modelling and precalculation presented herein is given to the comparison with detailed measurements from different already built machines.

2. Equivalent Circuits

As depicted in Fig. 1, the supplying voltage source inverter operates in either asynchronous or synchronous mode, in particular with higher fundamental frequencies. Regardless of the pulse pattern mode, the voltages applied to the machine and consequently the consumed currents are always non-sinusoidal with dominant fundamental harmonic components U_1, I_1 and various higher harmonic components U_k, I_k, $k = 1 + 6g$, $g \in \mathcal{Z}$. These non-sinusoidal quantities are further represented by Fourier series expansions using RMS values and initial phase angles of the respective harmonic components as

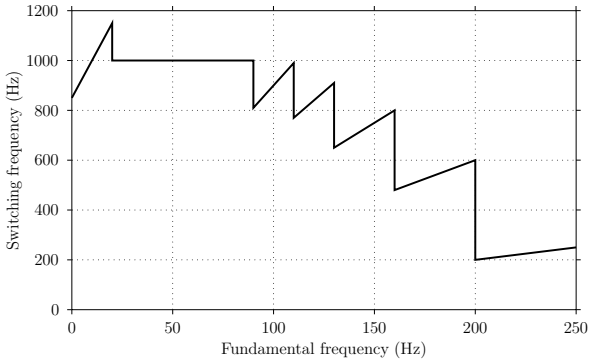

Fig. 1: Switching frequency versus fundamental frequency of a voltage source inverter of traction drives

$$U(\omega t) = \sum_k \sqrt{2}\, U_k \, \mathrm{e}^{\,j\varphi_{uk}} \, \mathrm{e}^{\,jk\omega t} \quad , \tag{1a}$$

$$I(\omega t) = \sum_k \sqrt{2}\, I_k \, \mathrm{e}^{\,j\varphi_{ik}} \, \mathrm{e}^{\,jk\omega t} \quad . \tag{1b}$$

Based on these Fourier series expansions, an equivalent circuit of each harmonic order k as depicted in Fig. 2 is introduced. The slip values s_k of the higher harmonics are obtained from the slip

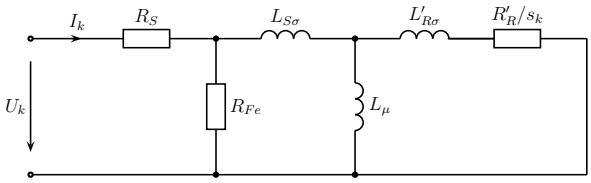

Fig. 2: Equivalent circuit for each harmonic component

of the fundamental component s_1 as

$$1 - s_1 = k\,(1 - s_k) \ . \tag{2}$$

With rated operational conditions, the slip of the fundamental component $s_1 \ll 1$ causes slip values of the higher harmonics $s_k \approx 1$. Consequently, the higher harmonics will generate additional losses which are approximately independent of the actual operational point [1], [3]. The parameters of each equivalent circuit are further calculated according to the following suggestions about iron and power losses.

3. Iron Losses

One important component of the additional losses concerned arises as iron losses caused by the higher voltage harmonics in particular in the stator and less significantly in the rotor laminations [3]–[5].

Basically, iron losses can be separated into three contributions of eddy current losses P_{ec}, hysteresis losses P_{hy} and excess losses P_{ex} [6]–[9]. Each of these three iron loss densities has its own dependence on frequency and magnetic flux,

$$\begin{aligned}
&\text{Eddy current losses:} && p_{ec} \sim f_k^2 \left(\frac{U_k}{f_k}\right)^2 \ , \\
&\text{Hysteresis losses:} && p_{hy} \sim f_k \left(\frac{U_k}{f_k}\right)^2 \ , \\
&\text{Excess losses:} && p_{ex} \sim f_k^{1.5} \left(\frac{U_k}{f_k}\right)^{1.5} \ .
\end{aligned}$$

In particular, the hysteresis losses are additionally influenced by the level of saturation caused by the fundamental harmonics when operating in either constant field or field weakening region.

The actual values of the iron losses are obtained from the geometry data as well as material dependent coefficients known from already utilized lamination sheets.

The magnetizing inductance of the fundamental harmonics can be evaluated in accordance with the magnetic characteristic of the entire machine for each operating point in either the constant field or field weakening region. Additionally, the level of saturation defines an appropriate differential magnetizing inductance representing the magnetization current of the higher harmonics.

4. Power Losses

The most important component of the additional losses concerned arises as power losses from higher current harmonics in the conductors of both stator and rotor windings [3]–[5]. Due to the high frequencies of these current components, the current displacement effects have to be considered in detail. Based on the well-known skin depth

$$\delta_C = \sqrt{\frac{2}{\omega \mu_0 \gamma}} \tag{3}$$

in dependence on circular frequency ω and conductivity γ [3], [4], [10], [11], a reduced slot conductor height or radius ξ and additionally a complex parameter ζ are defined as

$$\xi = \frac{h_C}{\delta_C} \quad \text{or} \quad \xi = \frac{r_C}{\delta_C} \ , \quad \zeta = \xi\,(1 + j) \ . \tag{4}$$

The skin effect significantly affects the impedance of slot conductors along the lengths of stator and rotor lamination stack.

4.1 Opened stator slots

Asynchronous induction machines of traction drives are always equipped with opened stator slots in order to carry the form-wound winding coils [12], [13]. Usually, there is an equal number of rectangular conductors in both upper and lower layers resulting in an even number n of slot conductors. By using DC resistance R_0 and inductance L_0 [11], the complex impedance of each of the n rectangular slot conductors is given by

$$\frac{Z_p(\zeta)}{R_0} = \zeta \left(\coth\zeta + 2p\,(p-1)\,\tanh\frac{\zeta}{2}\right) \ , \quad 1 \le p \le n \ . \tag{5}$$

The decomposition into real and imaginary parts yields

$$\begin{aligned}
k_{pR}(\xi) &= \frac{\operatorname{Re} Z_p(\zeta)}{R_0} \\
&= \varphi_R(\xi) + p\,(p-1)\,\psi_R(\xi) \ , \qquad \text{(6a)} \\
k_{pX}(\xi) &= \frac{\operatorname{Im} Z_p(\zeta)}{\omega L_0} \\
&= \varphi_X(\xi) + p\,(p-1)\,\psi_X(\xi) \qquad \text{(6b)}
\end{aligned}$$

with the real functions

$$\varphi_R(\xi) = \xi \frac{\sinh 2\xi + \sin 2\xi}{\cosh 2\xi - \cos 2\xi} \ , \tag{7a}$$

$$\psi_R(\xi) = 2\xi \frac{\sinh \xi - \sin \xi}{\cosh \xi + \cos \xi} \ , \tag{7b}$$

$$\varphi_X(\xi) = \frac{3}{2\xi} \frac{\sinh 2\xi - \sin 2\xi}{\cosh 2\xi - \cos 2\xi} \ , \tag{7c}$$

$$\psi_X(\xi) = \frac{3}{\xi} \frac{\sinh \xi + \sin \xi}{\cosh \xi + \cos \xi} \ . \tag{7d}$$

In dependence on the arrangement of the slot conductors with the end winding connection, averaged values of resistance and inductance are described as

$$k_{nR}(\xi) = \varphi_R(\xi) + m(n)\,\psi_R(\xi) \ , \tag{8a}$$

$$k_{nX}(\xi) = \frac{1}{n^2}\Big(\varphi_X(\xi) + m(n)\,\psi_X(\xi)\Big) \ . \tag{8b}$$

Therein, weighting factors

$$m(n) = \frac{n^2-1}{3} \quad \text{or} \quad m(n) = \frac{n^2-4}{6} \tag{9}$$

are introduced without or with transposition of the $n/2$ slot conductors in each layer, respectively [4].

In particular with the stator, the current displacement within the end winding region has to be considered. According to [3], [4], modified functions $\varphi'_R(\xi)$, $\psi'_R(\xi)$ and $\varphi'_X(\xi)$, $\psi'_X(\xi)$ yielding $k'_{nR}(\xi)$ and $k'_{nX}(\xi)$ can be defined. Finally, averaged resistance and inductance factors are obtained from

$$k_R(\xi) = \frac{k_{nR}(\xi)\,l_S + k'_{nR}(\xi)\,(l_W - l_S)}{l_W} \ , \tag{10a}$$

$$k_X(\xi) = \frac{k_{nX}(\xi)\,l_S + k'_{nX}(\xi)\,(l_W - l_S)}{l_W} \ , \tag{10b}$$

wherein l_S and l_W denote stacking length and half total length of one single winding, respectively.

4.2 Semi-closed rotor slots

In many cases, asynchronous induction machines of traction drives are equipped with unskewed semi-closed rotor slots containing rectangular or slightly trapezoidal slot conductors. By using the DC resistance R_0, the complex impedance of such slot conductors is given by

$$\frac{Z(\zeta)}{R_0} = \zeta^2 \left(\frac{\coth \zeta}{\zeta} + \sum_{n=1}^{\infty} 2 \left(\mathrm{si} \frac{n\pi s}{b_C} \right)^2 \frac{\coth \zeta_n}{\zeta_n} \right) \ ,$$

$$\zeta_n = \sqrt{\left(\frac{2n\pi h_C}{b_C} \right)^2 + \zeta^2} \ , \tag{11}$$

wherein s, b_C, h_C denote the width of the slot opening as well as width and height of the slot conductor, respectively [11].

In case of cylindrical slot conductors, the complex impedance of the slot conductors is obtained from

$$\frac{Z(\zeta)}{R_0} = \frac{\zeta}{2} \left(\frac{I_0(\zeta)}{I'_0(\zeta)} + \sum_{n=1}^{\infty} 2 \left(\mathrm{si}(n\alpha) \right)^2 \frac{I_n(\zeta)}{I'_n(\zeta)} \right) \ ,$$

$$\alpha = \arcsin \frac{s}{2r_C} \ , \tag{12}$$

wherein s, r_C denote the width of the slot opening as well as the radius of the slot conductor and I_n, I'_n are the modified Bessel functions of first kind and their derivates, respectively [11].

With the additional losses of the higher harmonics, the impact of various designs of the end winding region can be neglected.

5. Comparison with Measurements

5.1 Voltages and currents

Fig. 3 and Fig. 4 depict a comparison of measurement and simulation data for the phase voltage

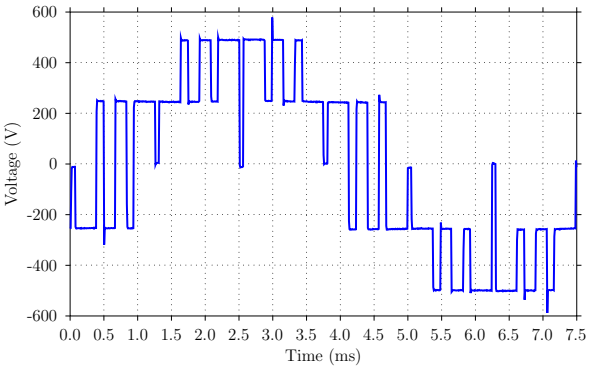

Fig. 3: Phase voltage with synchronous mode operation, measurement data

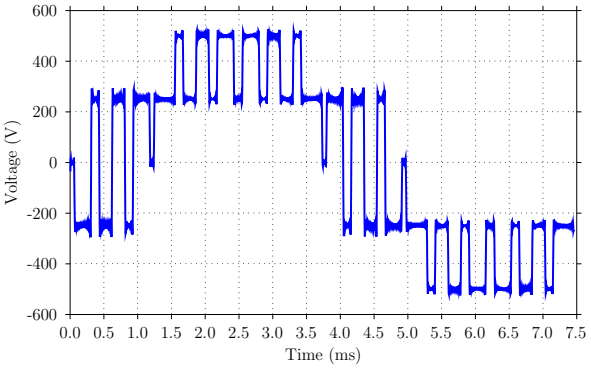

Fig. 4: Phase voltage with synchronous mode operation, simulation data

with a synchronous mode operation of the inverter. Fig. 5 and Fig. 6 depict a comparison of measurement and simulation data for phase voltage and phase current with the block mode operation of the inverter arising with high fundamental frequencies in the field weakening range. Obviously, the presented approximation by using an equivalent circuit for each harmonic component can represent the behaviour of these higher harmonics in an appropriate way.

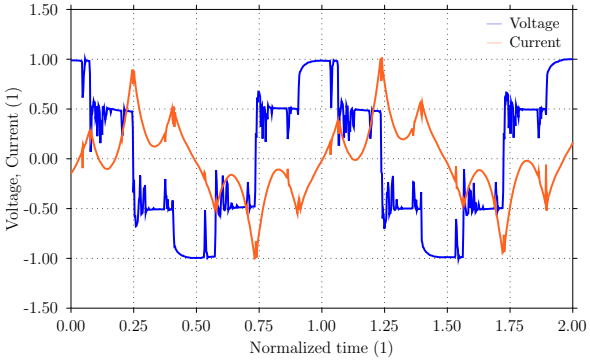

Fig. 5: Phase voltage and phase current with block mode operation, measurement data

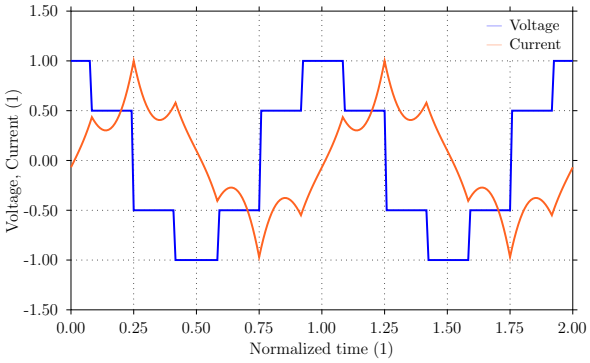

Fig. 6: Phase voltage and phase current with block mode operation, simulation data

5.2 Iron and power losses

The Fourier series expansions (1) of the non-sinusoidal voltages and currents result in the time-averaged power consumption

$$P = 3 \sum_k U_k \, I_k \, \cos\bigl(\varphi_{uk} - \varphi_{ik}\bigr) \ . \qquad (13)$$

Consequently, each of the harmonic components $k = 1+6g$, $g \in \mathcal{Z}$, produce their respective portion within the entire power consumption separately and independently of the other harmonic components. Thereby, the power

$$P_1 = 3 \, U_1 \, I_1 \, \cos\bigl(\varphi_{u1} - \varphi_{i1}\bigr) \qquad (14)$$

produced by the fundamental harmonic components denotes the fundamental power consumption.

Due to the slip values (2) of the higher harmonics, the power factor of the higher harmonic components is significantly smaller than the power factor of the fundamental harmonic components. Thus, in particular the evolved electromagnetic torque arises mostly from only the fundamental harmonic components.

Consequently, the additional losses caused by the inverter are obtained from two series of measurements. First, only sinusoidal terminal voltages according to the voltage-frequency characteristic of the inverter are applied to the machine with various load conditions. Secondly, the same load conditions are applied by using the inverter directly.

Fig. 7, Fig. 8 and Fig. 9 depict a comparison of measurement and simulation data for the additional losses caused by the inverter for a typical traction machine in dependence on the switching frequency of the inverter.

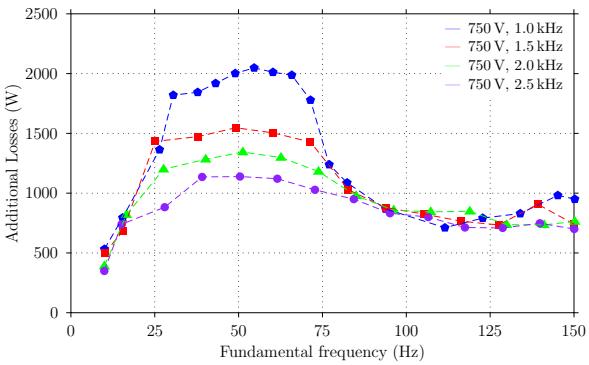

Fig. 7: Measurement data of additional losses caused by the inverter for an asynchronous induction machine of traction drives with a rated power of 100 kW in dependence on the switching frequency

As obtained from measurements, the switching frequency of the inverter significantly affects the total additional losses caused by the higher harmonic components. But an increased switching frequency of the inverter causes additional losses and subsequently thermal design problems with the inverter. In particular, an increased switching frequency of the inverter yields decreased additional losses in particular in the constant field region. On the other hand in the field weakening range, the additional losses are only slightly affected by the switching frequency of the inverter. Consequently, there are important fields of an optimization of both inverter and electrical machine in order to get an optimal behaviour of both components in terms of losses and efficiency.

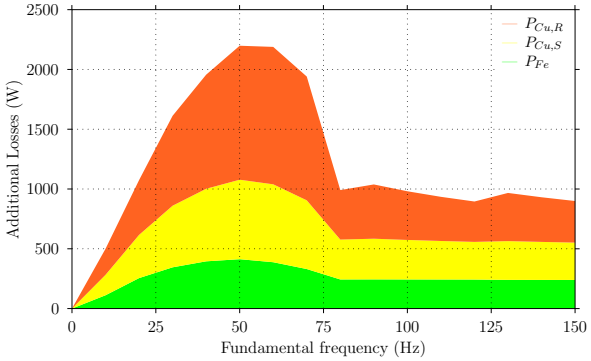

Fig. 8: Simulated main components of additional losses caused by the inverter for an asynchronous induction machine of traction drives with a rated power of 100 kW, switching frequency of 1 kHz

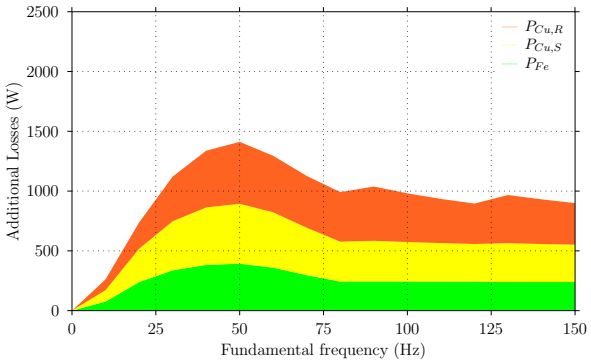

Fig. 9: Simulated main components of additional losses caused by the inverter for an asynchronous induction machine of traction drives with a rated power of 100 kW, switching frequency of 2 kHz

The comparison with the evaluated data obtained from equivalent circuits of the higher harmonics shows a good accordance. As expected, the most dominant part of the additional losses caused by the higher harmonics arises from the power losses within the rotor. All three main components of the additional losses increase with fundamental frequencies up to values approximately to the half of the constant field region. With higher fundamental frequencies in the upper constant field region, they decrease to smaller values. Finally, all three portions are approximately constant within the field weakening region.

6. Conclusion

In terms of additional losses caused by non-sinusoidal voltages and currents of the supplying voltage source inverter, asynchronous induction machines used with traction drives of rail transportation vehicles have to be treated differently than standard induction machines. Therefore, the paper discusses modelling and precalculation of iron and power losses additionally arising from the inverter to be suitable for a more accurate initial design of such machines. Special attention is paid to an inclusion of various components of the iron losses as well as an accurate evaluation of the current displacement in both stator and rotor slot conductors. The presented evaluation method based on Fourier series analyses of the terminal voltages is successfully compared with detailed measurement results obtained from already built machines.

References

[1] Kleinrath H.: *Stromrichtergespeiste Drehfeldmaschinen* (in German). Springer, Vienna, 1980.

[2] Beaty H.W., Kirtley J.L.: *Electric Motor Handbook*. McGraw-Hill Book Company, New York (USA), 1998.

[3] Pyrhönen J., Jokinen T., Hrabovcová V.: *Design of Rotating Electrical Machines*. John Wiley & Sons Ltd, Chicester (UK), 2008.

[4] Müller G., Vogt K., Ponick B.: *Berechnung elektrischer Maschinen* (in German). Wiley-VCH, Weinheim, 2008.

[5] Green T.C., Hernandez-Aramburo C.A., Smith A.C.: "Losses in Grid and Inverter Supplied Induction Machine Drives". *IEE Proceedings Electrical Power Applications*, Vol. 150, No. 6, November 2003.

[6] Boglietti A., Chiampi M., Repetto M., Bottauscio O., Chiarabaglio D.: "Loss Separation Analysis in Ferromagnetic Sheets Under PWM Inverter Supply". *IEEE Transactions on Magnetics*, Vol. 34, No. 4, July 1998.

[7] Pippuri J., Arkkio A.: "Time-Harmonic Induction Machine Model Including Hysteresis and Eddy Currents in Steel Laminations". *IEEE Transactions on Magnetics*, Vol. 45, No. 7, July 2009.

[8] Dlala E., Arkkio A.: "A General Model for Investigating the Effects of the Frequency Converter on the Magnetic Iron Losses of a Squirrel-Cage Induction Motor". *IEEE Transactions on Magnetics*, Vol. 45, No. 9, September 2009.

[9] Boglietti A., Cavagnino A., Ionel D.M., Popescu M., Staton D.A., Vaschetto S.: "A General Model to Predict the Iron Losses in PWM Inverter-Fed Induction Motors". *IEEE Transactions on Industry Applications*, Vol. 46, No. 5, September 2010.

[10] Field A.B.: "Eddy currents in large slot-wound conductors". *Transactions of the American Institute of Electrical Engineers*, Vol. 24, January 1905.

[11] Schmidt E.: *Stromverdrängung in Nutenleitern* (in German). Master Thesis, Vienna University of Technology, 1985.

[12] Islam M.J., Arkkio A.: "Effects of Pulse-Width Modulated Supply Voltage on Eddy Currents in the Form-Wound Stator Winding of a Cage Induction Motor". *IET Electric Power Applications*, Vol. 3, No. 1, January 2009.

[13] Islam M.J., Khang H.V., Repo A.K., Arkkio A.: "Eddy Current Loss and Temperature Rise in the Form-Wound Stator Winding of an Inverter Fed Cage Induction Motor". *IEEE Transactions on Magnetics*, Vol. 46, No. 8, August 2010.